Hydrothermally Fabricated Bio-nanocomposite of Guar gum as a Promising Adsorbent for Reactive Green 19 Dye from Wastewater

Laishram Saya[a,b,c], Sunita Hooda[b], W. Rameshwor Singh[a,*]
[c]*Department of Chemistry, Manipur University, Canchipur, Imphal-795003, Manipur, India*
[b]*Polymer Research Laboratory, Department of Chemistry, Acharya Narendra Dev College (University of Delhi), Govindpuri, Kalkaji, New Delhi – 11 0 019, India*
[c]*Department of Chemistry, Sri Venkateswara College (University of Delhi), Dhaula Kuan, New Delhi-110021, India*

***Abstract*-Reactive dyes which are mainly used for dyeing cotton and other cellulose-based fibers are released in huge quantities into water bodies. They are associated with several harmful effects including allergic dermatoses, respiratory diseases, colonic and rectal cancers, etc. In this paper, we report a novel and facile synthesis of bio-nanocomposite of magnetic guar gum (BMGG) wherein the polymeric network of guar gum is decorated with spinels of magnetic nanoparticles via a simple hydrothermal method which shows promising removal efficiency for reactive dyes. Physicochemical techniques such as FESEM, TEM, EDAX, FTIR, Raman, TGA, VSM, $pH_{ZPC,}$ and XRD have been used for characterizing the as-synthesized nanocomposite. Batch adsorption studies carried out on BMGG showed rapid and excellent adsorption potential of the semi-synthetic material exhibiting a removal efficiency of up to 98.44 % within an hour with a maximum adsorption capacity of 526.32 mg g^{-1} for anionic Reactive green 19 dye from aqueous medium. The adsorption kinetics data fitted best into the pseudo-second-order model. Out of various isotherm models being studied such as Langmuir model, Freundlich and Temkin model, the adsorption equilibrium was found to be best described by the Langmuir isotherm model. The spontaneous as well as the exothermic nature of the adsorption phenomenon, is clearly evident from the thermodynamic studies. BMGG composites also showed significant regeneration capacity showing retention in adsorption efficiency even up to several cycles of adsorption-desorption process. Hence, the reported semisynthetic nanomaterial holds a good scope of playing a significant role in solving the perpetual challenge of water pollution.**

Keywords: **adsorption, kinetics, isotherms, reactive green 19, adsorption capacity**

1. INTRODUCTION

Over the last 10 years, researchers from various domains have been putting in relentless efforts in the field of exploration and design of sustainable materials that can be utilized as adsorbents for the removal of toxic contaminants from wastewater, most importantly synthetic dyes. Among several categories of dyes, being synthesized, Reactive dyes are the ones that are used on an extensive scale. A Reactive dye primarily has chromophores containing an azo or anthraquinone moiety along with a number of other reactive groups such as an activated double bond (e.g., vinyl sulphone) or a, heterocycle (e.g., trichloropyrimidine, chlorotriazine or difluorochloropyrimidine) (Mahmoud et al., 2007). Reactive dyes, owing to a multitude of advantages such as chemical stability, easy accessibility, fast and facile binding with the fabric, have been used on large scale for coloring cellulosic/cotton fabric. Due to their chemical stability and high solubility in aqueous medium, these dyes are non-biodegradable due to which they pass untreated from the effluents through most of the conventional treatment methods (Özacar et al., 2013). Various basic parameters such as temperature, salt concentration, and alkaline condition along with the reactivity and diffusion coefficient of the dye play a crucial role in determining the dye fixation efficiency of reactive dyes on cellulosic fabrics (Hossain et al., 2020, Lee et al., 2019). Nevertheless, the efficiency of dye fixation on cellulosic fibers is considerably low varying from only 50-90%, which results in low absorption of these dyes on the fabrics. This, in turn, leaves a high content

of dye in the supernatant giving an intensely colored effluents which are subsequently disposed of recklessly into water bodies, and enters the food chain through groundwater posing an alarming threat to the environment (Cooper et al., 1995, Lewis et al., 1993). Due to their ability to screen sunlight, these dyes hinder photosynthesis and lower dissolved oxygen levels (Durairaj et al., 2019). They are even proven to be related to mutagenic and carcinogenic effects (Saya et al., 2021). It is also worth mentioning that the high amounts of electrolyte (40–100 g/L) and alkali (5–20 g/L) being used for cellulose fiber dyeing may also be responsible for other effluent issues. Hence, environmental contamination caused by reactive dyes has become more and more severe with the ever-escalating use of reactive dyes.

There have been persistent efforts over the last few decades to discover sustainable and economical materials as well as more efficient methods for the sequestration of these harmful dyes from wastewater. Among several techniques meant for wastewater remediation, adsorption has most extensively by virtue of its beneficial characteristics, including its high removal efficiency, low cost, ease in handling, and minimal complexity in design. (Arabi et al., 2016; Bagheri et al., 2019). Apart from the exploration of superior and novel removal methods for water clean-up, researchers have been working diligently on the design of sustainable materials with high surface areas and improved adsorption efficacy (Alshahrani et al., 2022; You et al., 2022; Do et al., 2022). Natural polysaccharides, such as Guar gum, serve as one of the most viable candidates in this field owing to several beneficial characteristic properties including their prevalence in nature, affordability, and most importantly eco-friendly nature (Saya et al., 2021). Guar gum has plenty of hydroxyl groups in its polymeric backbone that can undergo extensive hydrogen bonding in aqueous medium, which is further enhanced by the single-membered galactose branches as well as the mannose units (as shown in Fig. 1 (a)). Through batch adsorption studies, the effect of various parameters such as temperature, pH, contact time and concentration of Reactive Green 19 dye was investigated, chemical structure of which is shown in Fig. 1 (b). These equilibrium experimental data when fitted into different kinetic and isotherm models showed that the adsorption of RG 19 on BMGG could best be explained by pseudo second-order model and Langmuir isotherm model. An analysis of the recyclability data reveals good reusability property of BMGG with significant retention in removal efficiency toward RG 19 after several batches of adsorption-desorption analysis.

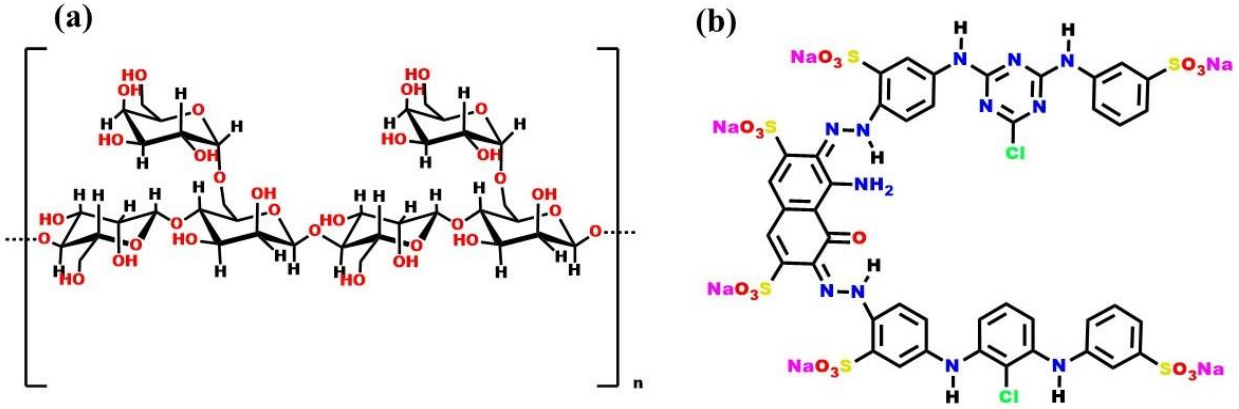

Fig. 1. Chemical structure of (a) Guar gum polysaccharide and (b) Reactive Green 19 Dye

2. MATERIALS AND METHODS

2.1. Materials. All reagents which were used for synthesis and other procedures were of analytical grade and used without any further purification. Guar gum (99%), Ferrous chloride (96.0%), Ferric chloride (96.0%), Reactive Green 19 Dye (λmax = 630 nm), Sodium Hydroxide (97%), Hydrochloric acid (35%), Ammonia solution (30 wt %), were purchased from Merck. Double Distilled water was used for the preparation of standard solutions of dye as well as other experimental procedures.

2.3. Synthesis of BMGG.

The bio-nano composite of guar gum (BMGG) was successfully fabricated by a facile hydrothermal

process. 0.5g of guar gum was dissolved in 50 ml distilled water and sonicated for 30 minutes. 2 g ferric chloride and 5.2 g of ferrous chloride were dissolved in 50 mL of water which was mixed with the above presonicated GG solution. The reaction mixture was then placed inside a 100 ml Teflon lined stainless steel autoclave for hydrothermal process and heated for 2 hours at 80°C. It was then allowed to cool down slowly to room temperature followed by the addition of 3-4 ml of ammonia solution dropwise with continuous stirring. The nanocomposite of BMGG gets precipitated out as black colored solid which was washed with distilled water several times to bring to neutral pH, and finally dried in a vacuum oven. It was finally ground into fine powder. Fig. 2 gives the stepwise schematic representation of the whole synthesis procedure.

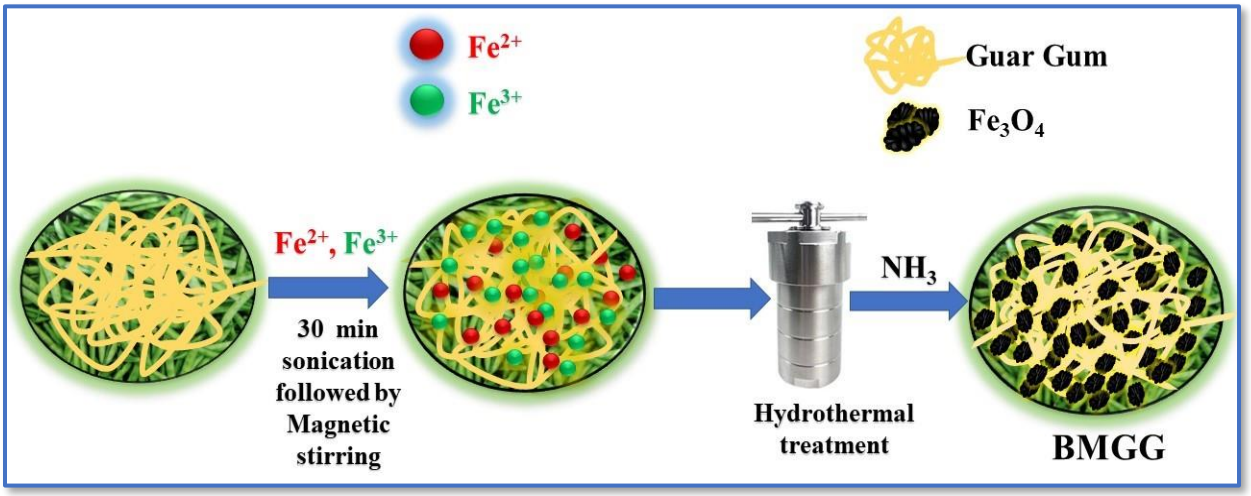

Fig. 2. Schematic depiction for hydrothermal synthesis of BMGG

2.4. Characterization of BMGG

The as-synthesized bio nanocomposite was characterized with the help of various physico-chemical techniques. The X-ray powder diffraction (XRD) spectra were recorded with PANalytical, X'Pert PRO X-ray diffractometer at room temperature using Cu Kα X-ray radiation source with a wavelength of 154 Aº. The Raman spectra at 25 °C were recorded using Renishaw Insvia II Raman spectrometer equipped with a laser that works at 514 nm wavelength. The Fourier transform infrared (FTIR) spectra were obtained from a Thermo Fisher NICOLET IS50 FTIR spectrometer wherein KBr pellets were used in the wavenumber range 400−4000 cm^{-1}. For surface morphological analysis, Field Emission Scanning Electron microscope (FESEM) images were taken with the help of a Zeiss Gemini 500 Field Emission Scanning Electron Microscope that provides nanoscale images starting from 100 mm diameter. Also, high-resolution transmission electron microscopy (HRTEM) images of the nanocomposites were obtained from FEI Tecnai TF20 high resolution Transmission Electron Microscope (TEM) equipped with a field-emission gun (FEG). The magnetic moment of the sample was analyzed at 300 K using a Vibrating Sample Magnetometer (VSM) that works on a Microsensor, Model ADE-EV9. For thermal characterization, Thermo- Gravimetric Analysis (TGA) was carried out using TGA HiRes1000 which has a heating rate of 0.01 to 200 °C/min

2.5. Application of BMGG for Dye Adsorption.

In order to analyze the dye adsorption behavior of BMGG on RG 19 dye, a series of batch adsorption studies were performed. The overall adsorption efficiency of the composite was optimized through the investigation of various parameters such as temperature, pH, contact time, initial dye concentration and adsorbent dosage. The maximum adsorption capacity was determined under optimized conditions of temperature of 298 K, taking 5 mg of BMGG into 5 mL of dye solution (4 mM) at pH 8 and 9 for RG 19, respectively. Each time, after the dynamic equilibrium adsorption was reached, the adsorbent was removed from the solution with the help of an external magnet and the absorbance of the supernatant dye

solution after adsorption was measured with the help of a UV-Visible spectrophotometer at the corresponding λ_{max} value of 630 nm.

For exploring the standards and quality of BMGG two important properties of the adsorbent; equilibrium adsorption capacity q_e (in mg g^{-1}) is expressed as the amount of dye adsorbed on the surface of unit mass of an adsorbent and removal efficiency which is expressed in terms of the percentage of pollutant removed with reference to the initial concentration were evaluated, which are given by equations 1 and 2 respectively.

$$q_e = \left(\frac{(C_o - C_e)V}{m}\right) \quad (1)$$

$$\text{removal efficiency } (\%) = \frac{C_o - C_e}{C_o} \times 100 \quad (2)$$

where, C_o is the initial dye concentration (mg/L), C_e is the remaining dye concentration in the solution at time (t), V is the volume of the dye solution used (in L), and m is the mass of the adsorbent used (in g).

3. RESULTS AND DISCUSSION

3.1. XRD analysis and structural properties:

The XRD spectra of Fe_3O_4 nanoparticles and BMGG along with that of neat guar gum (as inset) are shown in Fig 3(a). Almost all the characteristic peaks corresponding to 2θ = 30.1° (2 2 0), 35.5° (3 1 1), 43.2° (4 0 0), 53.6° (4 2 2), 57.2° (5 1 1), and 62.7 ° (4 4 0) are observed in the spectra of Fe_3O_4 nanoparticles (Noval et al., 2019) which also appear in that of BMGG, however with lesser intensity. This confirms the successful and effective incorporation of Fe_3O_4 nanoparticles in BMGG. As can be seen from the XRD spectrum of neat guar gum, characteristic peaks appear at 17.47◦ and 20.12◦ indicative of its semicrystalline nature (Mudgil et al., 2012). However, in the case of BMGG, we can observe the appearance of a strong and broad new peak at 14.5º along with the disappearance of the characteristic peaks of GG which may possibly be due to the destruction of the semi-crystalline property of GG. Inference can be drawn from these observations that the decoration of GG with Fe_3O_4 nanoparticles leads a significant modification in the chemical structure of GG that might have subsequently led to the enhancement of adsorption capability of BMGG as compared to neat GG.

3.2. Chemical properties analysis (FTIR, RAMAN, VSM)

The presence of various functional groups in the as-synthesized nanocomposites was confirmed through a careful comparative analysis of the FTIR spectra of pure GG, Fe_3O_4 nanoparticles and BMGG which are shown in Fig. 3 (b). In the FTIR spectra of BMGG, two strong absorption bands appearing at around 634, 589 and 450 cm^{-1} are observed, which are missing in that of pure GG. The peak at around 589 cm^{-1} is mainly attributed to the Fe-O stretching vibration at the tetrahedral sites of Fe_3O_4 spinel structure (Li et al., 2015), while another small peak at cm^{-1} can be assigned to Fe-O stretching at the octahedral sites (Pati et al., 2013) This clearly confirms the successful doping of Fe_3O_4 nanoparticles in the GG network. Apart from this several characteristics peaks of pure guar gum are retained in the FTIR spectrum of BMGG. However, a red (bathochromic) shift is observed in the peak corresponding to the O-H stretching that appears at 3403 cm^{-1}, while it is visible at 3320 cm^{-1} in pure GG, which may be due to the weakening of the original bonds after being doped with magnetite nanoparticles. Besides, the following peaks are also observed in both FTIR spectra of BMGG and GG: 2927 cm^{-1} correspond to stretching vibration mode of C–H of the CH_2 group; 1650 cm^{-1} suggesting the presence of carbonyl C=O group and its stretching mode and 1016 cm^{-1} assigned to C-O stretching frequency.

However, many of characteristics peaks that are visible in pure GG spectrum are found to be disappeared in that of BMGG, such as the peaks at 1068 cm^{-1} that represents C-O-C stretching in the anhydroglucose ring, absorption bands between 871−813 cm^{-1} due to the galactose and mannose moieties and 1417 cm^{-1} characteristic of C-H bending mode (Balan et al., 2019). The disappearance of these peaks suggests the fact that the chemical structure of guar gum is greatly modified due to the grafting of Fe_3O_4 nanoparticles which is also in corroboration with the results obtained from XRD analysis.

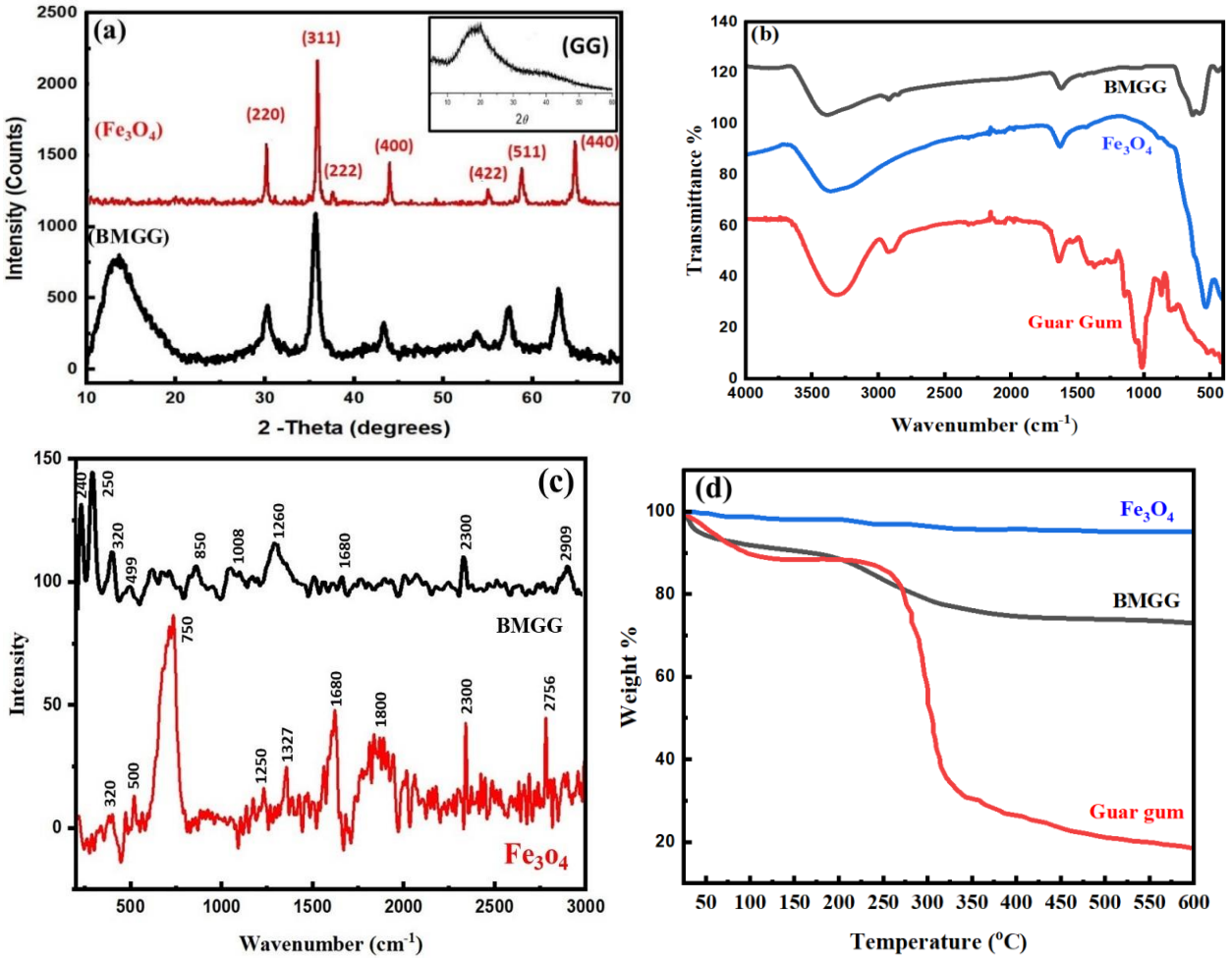

Fig. 3 (a) XRD spectra (b) FTIR spectra (c) Raman spectra and (d) TGA curves for pure Guar gum, Fe_3O_4 and BMGG

In order to gain more insight of the structure of BMGG, comparative analysis of its Raman spectra with those of its precursors is being carried out. As shown in Fig. 3 (c), the Raman band in the region of 850-1010 cm^{-1}, corresponding to the skeleton mode of the anomeric skeletal configuration (a or b conformers) ascribed to C–C or C–O vibrations coupled with the C–H mode of the anomeric carbon of b-conformers (Malfait et al., 1989). In case of Fe_3O_4 nanoparticles, characteristic peak with highest intensity is observed at 750 cm^{-1} which is missing in the case of BMGG while peaks at 1250, 1680, 2300, 2756 cm^{-1} are still retained with a little shift toward the higher wavelength side which is indicative of the weakening of the original bonds after the composite formation with Fe_3O_4

Since, the synthesis involves the addition of Fe_3O_4 nanoparticles, the material is expected to be magnetic. The inheritance of magnetic property in BMGG was investigated with the help of VSM technique at room temperature and the magnitude of magnetization curve of guar gum decorated with Fe_3O_4 is shown in Fig 4 (i). The curve shows no appearance of hysteresis loops and coercivity which gives inference about the superparamagnetic nature of BMGG. The saturation magnetization value at room temperature was found to be 39 emu/g, a value that is less than that of bulk Fe_3O_4 (92 emu/g) (Cao et al., 2008).

3.3. Morphological analysis (FESEM, TEM, EDAX)

Analysis of FESEM and TEM images is relatively a useful technique for the prediction of surface morphology as well as particle size or shape. Fig. 4 (a-b), 4 (c) and 4 (d-f) respectively show the FE-SEM images of pure guar gum, Fe_3O_4 nanoparticles and the

synthesized BMGG for the magnifications as shown. As can be seen from the images, pure guar gum is characterized by a smooth and homogeneous surface morphology. However, as a result of the doping process, the whole surface of GG becomes uniformly decorated with Fe_3O_4 nanoparticles that may be strongly binding with the oxygen containing functional groups of guar gum, thereby inducing a strong magnetic property to the nanocomposite. Furthermore, the surface of GG also appears to be crumpled and exist in fragmented form unlike that of pure GG. Images with higher magnification are able to highlight the spherical shape of the nanosized magnetite particles. Interestingly, the Fe_3O_4 nanoparticles are also more evenly distributed on the GG surface as compared to the pure Fe_3O_4 in which the particles appear to be in agglomerated form. A morphology well consistent with the results predicted above from FE-SEM images is also revealed by the HRTEM images of BMGG as shown in Figures 5 (a-c). A combined effect of all these morphological modifications must have led to enhanced adsorption performance for BMGG. The information about distribution of various constituent elements as well as the relative % content of these elements over a chosen area of the nanocomposite can be obtained from Energy Dispersive Analysis X-Ray (EDAX) analysis. The combined elemental mapping for O, Fe and C as well as elemental mappings for individual species over a specific area are shown in Fig. 5(d-g). In the EDAX survey spectra shown in Figure 5 (h), strong peaks of Fe and O can be seen. As per the data obtained, the compositions of the Fe, C and O have mass percentages of 53, 36 and 11% respectively.

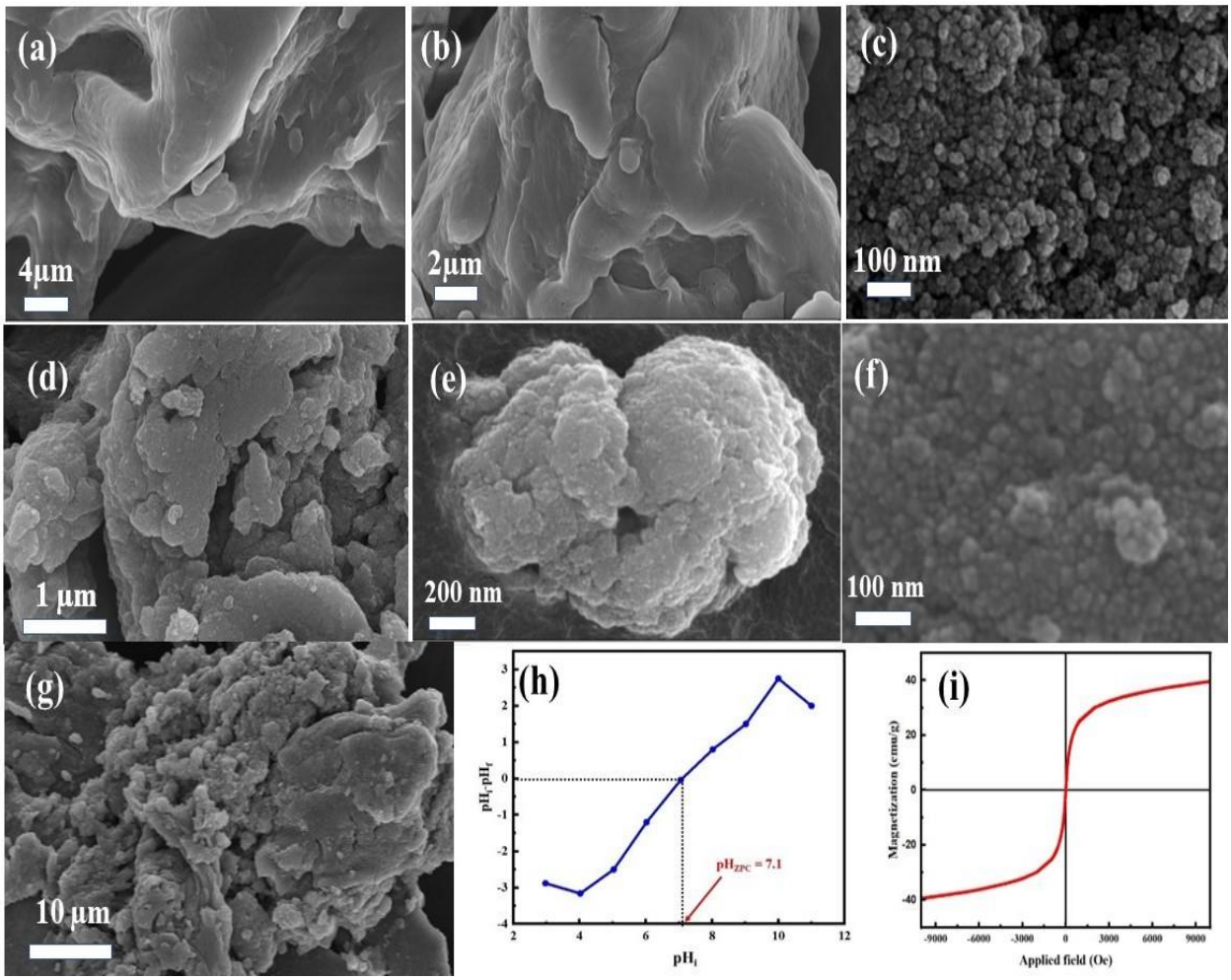

Fig. 4. FESEM images of (a-b) pure Guar gum (c) Fe_3O_4 (d-g) BMGG at different magnifications (h) curve for determining pH of Zero-point charge (i) Magnetization curve of BMGG

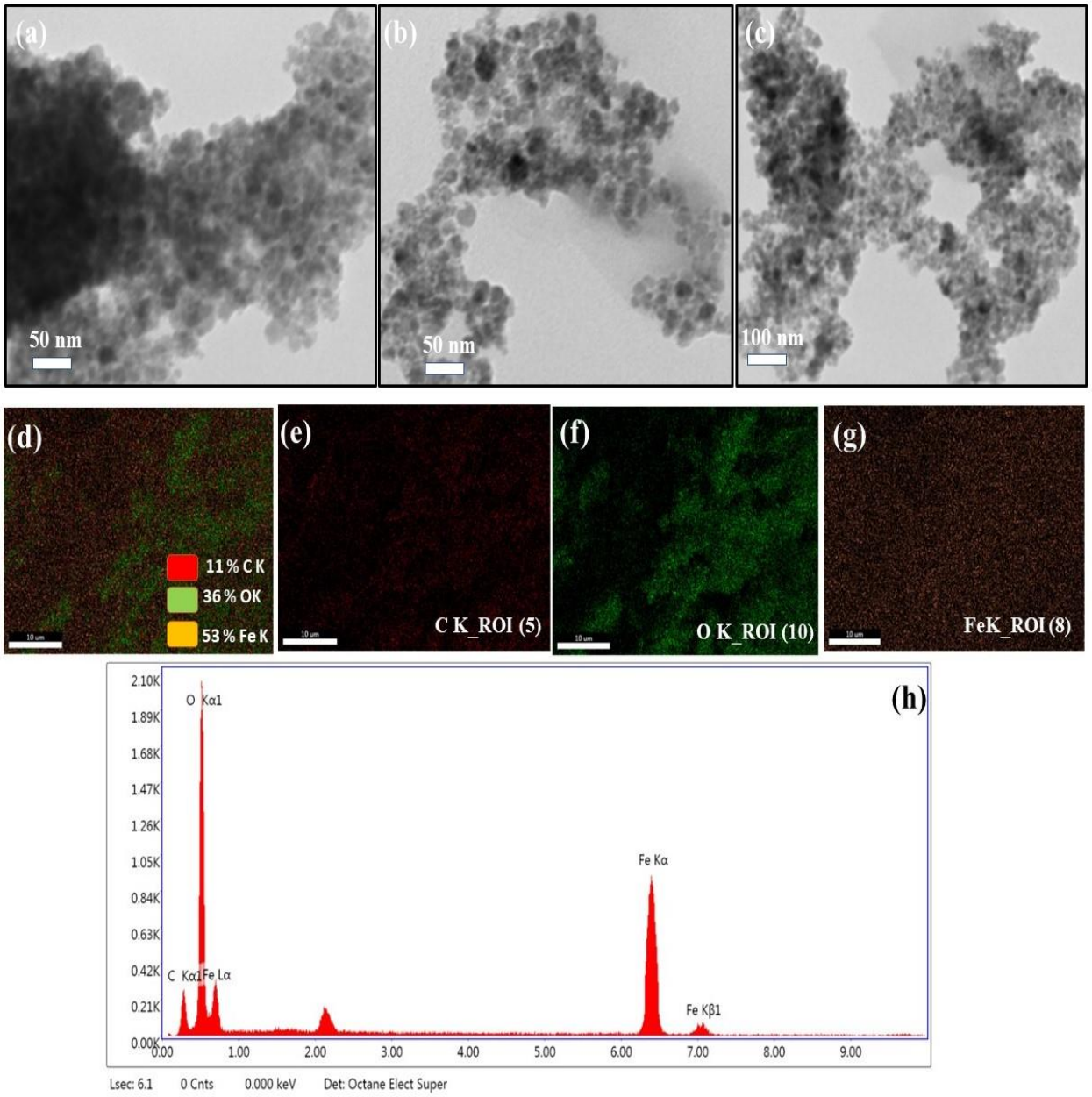

Fig. 5. HRTEM images of BMGG at varying magnifications (d-g) EDAX elemental mapping and (h) EDAX Sum Spectrum for the various elements present in BMGG.

The nature of charge developed on the material surface can be predicted through Zero-point charge (ZPC) analysis, which may further be of assistance in establishing a plausible mechanism for the adsorption phenomenon. At a particular pH called the pH_{ZPC} (pH of zero-point charge), the surface of the adsorbent becomes free of any charge. As per literature, the surface of an adsorbent is expected to be positively charged if the pH is less than pH_{ZPC} and negatively charged if greater (Liu et al., 2021). For determining pH_{ZPC}, a procedure reported in literature (Borousan et al., 2019) is followed wherein 10 ml KNO_3 solution (0.2 M) was taken in different viols to which HCl (0.5 N) and NaOH (0.5 N) were added in various aliquots to get the initial pH. To each viol was added 0.01 g of BMGG, kept on shaking for 24 hours after which the final pH was measured. The difference between the initial and final pH is plotted with respect to the corresponding initial pH, from which pH_{ZPC} was determined, as shown in Fig. 4 (h). pH_{ZPC} for BMGG

is obtained at pH=7.1, a value much higher than the pH at which BMGG exhibits maximum adsorption. This is in concordance with our experimental result that BMGG possesses excellent adsorption efficacy for anionic dyes on account of its positively charged surface.

3.4. Thermo-Gravimetric Analysis (TGA)

Thermogravimetric analysis (TGA) was carried out for neat guar gum GG, Fe_3O_4 nanoparticles and BMGG from 25 to 600ºC and the corresponding TGA curves are shown in Fig 3 (d). TGA thermograph of pure GG reveals that an initial weight loss occurs in the temperature range of 25-96ºC, the main reason for which is the evaporation of water molecules (Narayanamma et al., 2026). However, the major weight loss is observed in the temperature range of 270 to 335 ºC, at which the decomposition of guar gum takes place. In case of magnetite loaded GG, an initial weight loss occurs in short temperature range of 25-40ºC and the second step of weight moss is observed between 180-320ºC. It is important here to mention that a lowering of the second decomposition temperature is observed in BMGG as compared to pure GG which proves that the later to be more thermally stable. The enhanced thermal stability of BMGG is also distinctly evident from the total weight loss data as pure GG loses almost 80% of its weight at 600ºC while BMGG retains almost 72% of its weight (only 28% weight loss) at the same temperature. On the other hand, Fe_3O_4 nanoparticles shows only up to 2% weight loss.

4. ADSORPTION STUDIES

4.1. Adsorption Parameters

Significant role is being played by several parameters such as temperature, pH, time of contact, adsorbent dosage and concentration of dye solution in affecting the behavior of dye adsorption in aqueous medium. Thus, a careful analysis of how each parameter influences the adsorption process is of prime importance. Varying a parameter (say temperature) while keeping the rest of the parameters such as initial concentration of dye, amount of adsorbent, time, and pH constant, allows us to monitor the effect of that specific parameter on the adsorption behavior of the adsorbent toward a particular contaminant.

4.1.1. Effect of pH.

pH of the medium plays the most crucial role in influencing the adsorption behavior as pH can alter the net surface charge on the adsorbent material. Hence, the nature of interaction between the nanocomposite and the dyes molecules can be directly affected by pH and ultimately the selectivity toward a particular type of dye (cationic or anionic) is also affected. To study the effect of pH, the adsorption is monitored at various pH values as shown in Fig. 6 (a) within a fixed range taking optimized values of time, initial concentration of dye and adsorbent dosage and the trend of change in the adsorption capacity is analyzed. At $pH = pH_{ZPC}$ which is called the pH of Zero Point Charge, the surface of the adsorbent becomes electrically neutral. The $pH_{ZPC.}$ for BMGG was observed at 7.1 pH.

4.1.2. Effect of Concentration

The adsorption process at a particular temperature is greatly driven by the concentration gradient that develops between the nanocomposite surface and the dye. Hence, the concentration of the dye has great role to play with the concentration gradient. Investigation of this is usually carried out by an analysis of the variation trend in adsorption capacity with the change in initial dye concentrations at different temperatures. As shown in Fig. 6 (b), initially the adsorption capacity increases linearly with a regular increase in initial dye concentration until it reaches equilibrium at and beyond which no further increase in adsorption capacity is seen.

4.1.3. Effect of Contact Time

Monitoring the variation of adsorption capacity as a function of time is one of the most important analyses in studying the adsorption behavior of the adsorbent. Initially, the adsorbent shows a rapid increase in the adsorption of the dye till the equilibrium is reached after which the rate decreases gradually. This may be attributed to the presence of more vacant sites on the adsorbent surface in the initial adsorption stage which gradually get occupied with dye molecules as the adsorption progresses. Repulsive forces may in turn get developed amongst the adsorbed dye molecules which may account for the retardation in the speed of the adsorption. The adsorption data obtained with variation of time is helpful in studying the kinetics of the adsorption phenomenon.

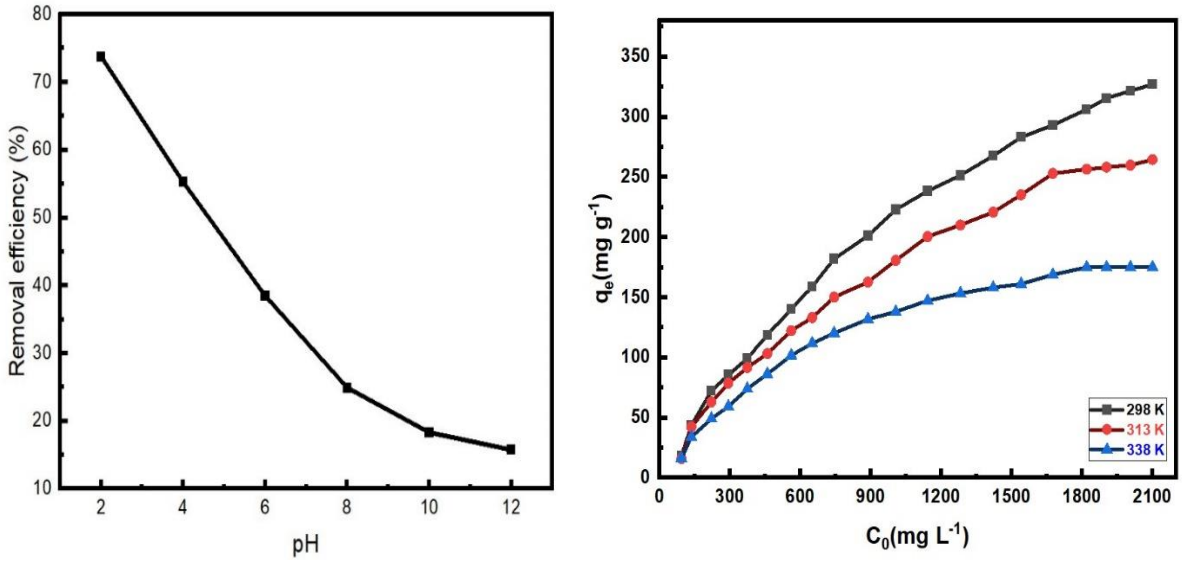

Fig. 6. (a) Variation of uptake capacity of BMGG with (a) pH (b) temperature and initial concentration of RG 19 dye.

4.2. Adsorption Kinetics.

The nature of variation of adsorption with duration of contact time gives useful information on the adsorption behavior (Verma et al., 2021). The kinetic studies of BMGG toward RG 19 was investigated making use of three types of kinetics models, i.e., Lagergren's pseudo-first-order, second-order and the Intra-particle diffusion model given by equations 3,4 and 5 respectively. The first order model gives inference of only physical interactions between the adsorbent and the adsorbate molecules unlike the second order model that indicates chemisorption of the adsorbate molecules onto the active sites of the adsorbent. On the other hand, the intra-particle diffusion model works on combination of three successive steps, (i) mass transfer across the external boundary layer film of liquid; (ii) rapid adsorption on the adsorbent surface (physical or chemical) and (iii) diffusion of the adsorbate molecules to an adsorption site, which is usually the rate controlling step.

$$ln(q_e - q_t) = lnq_e - K_1 t \quad (3)$$

$$\frac{t}{q_t} = \frac{t}{q_e} + \frac{1}{K_2 q_e^2} \quad (4)$$

$$q_t = k_i t^{0.5} + C \quad (5)$$

where q_e (in mg/g) and q_t (in mg/g) are the adsorption capacity at equilibrium and time t (in min), respectively. K_1 is the pseudo-first-order rate constant (in min^{-1}), and K_2 is the pseudo-second-order rate constant (in g mg^{-1} min^{-1}). The linear fit of the experimental kinetics data for all three kinetic models are illustrated in Fig. 7 (a-c), while Fig. 7(c) depicts the cumulative non-linear fit for all. Simultaneously, kinetic parameters associated with each model have been evaluated the above equations, results of which are listed in Table 1. As evident from the table, the pseudo-second-order model, and the straight fit lines have regression coefficient (R^2) values of 0.99588 for RG19. As illustrated in Fig. 7 (c), out of the three models investigated, the pseudo second-order model shows the best fit of the experimental results with theoretical calculations. This gives inference of the fact that the adsorption phenomenon of RG 19 dye on BMGG surface can be best represented by the pseudo second order model and is driven by chemical interactions between the two.

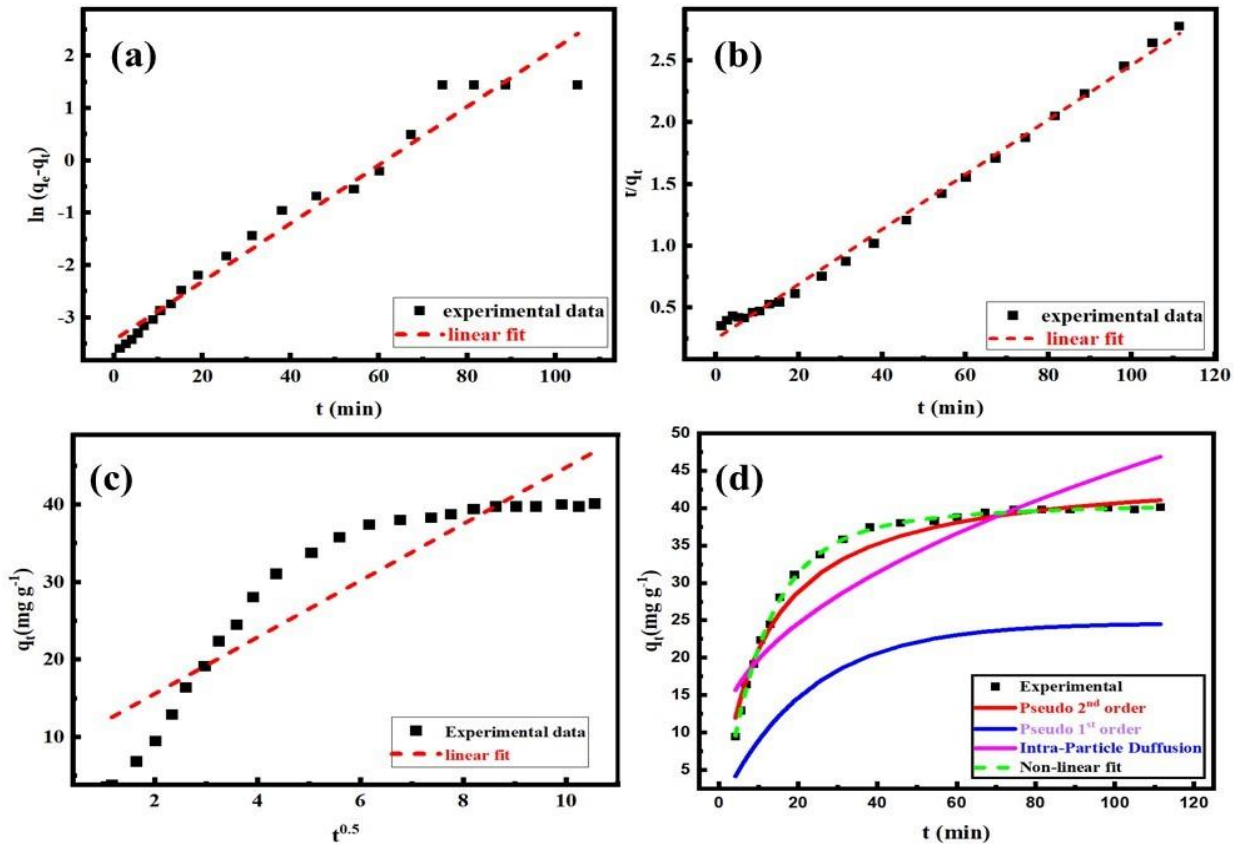

Fig. 7. Experimental data fit into (a) pseudo-first-order (b) pseudo-second-order and (c) Intra-particle Diffusion models (d) Combined Non-linear data fit into all three kinetic models.

Table 1: Kinetic parameters calculated for Pseudo-First-Order, Pseudo-Second-Order and Intra-Particle Diffusion Kinetic Models for the Adsorption of RG 19 dye on BMGG.

Model	Parameter	Value
Pseudo first order	q_e	24.655
	K_1	0.0454
	R^2	0.96775
Pseudo second order	q_e	45.248
	K_2	0.0195
	R^2	0.99588
Intra-particle Diffusion		0.82648
Experimental	K_{IPD}	3.6521
	C	8.3049

4.3. Adsorption Isotherm

In an attempt to study the interactions between BMGG and RG 19 dye, three isotherm models have been studied namely Langmuir, Freundlich and Temkin isotherm models (Banisheykholeslami et al., 2021; Gemici et al., 2021) using equations 6, 7, and 8 respectively. The adsorption behavior was checked starting with various initial concentrations of RG 19 dye.

$$q_e = \frac{q_{max} K_L C_e}{1 + K_L C_e} \quad (6)$$

$$q_e = K_F C_e^{1/n} \quad (7)$$

$$q_e = B ln(A_T C_e) \quad (8)$$

where q_e (in mg/g) and q_{max} are respectively the adsorption capacity at equilibrium and maximum adsorption capacity of the adsorbent at the equilibrium concentration C_e (in mg/L). The Langmuir adsorption constant, K_L (in L/mg) is related to the affinity of binding sites. In the Freundlich isotherm, the Freundlich isotherm constants K_F (in L/mg) and n are both related to the adsorption capacity. K_T (in L/mg) Temkin isotherm constants, which is related to the heat of adsorption. Adsorption isotherms studies toward RG 19 were carried out at temperatures of 298, 313, and 338 K and the rest of the experiments were carried out at 298 K. The experimental values were fitted into Langmuir, Freundlich and Temkin, adsorption models. The individual linear fit for the equilibrium

adsorption data as well as the combined non-linear fit into the three isotherm models are shown by Fig. 8(a-c) and 8(d) respectively. The regression coefficient (R^2) values were calculated for each adsorption model along with the corresponding adsorption constants listed in Table 2. Results indicate that Langmuir isotherm model with a R^2 value of 0.9955, show the best fit and can best describe the adsorption behavior of RG 19 on BMGG. This is indicative of only monolayer adsorption of the dye on magnetic guar gum with a maximum adsorption capacity (q_{max}) values of 526.31 mg g^{-1}.

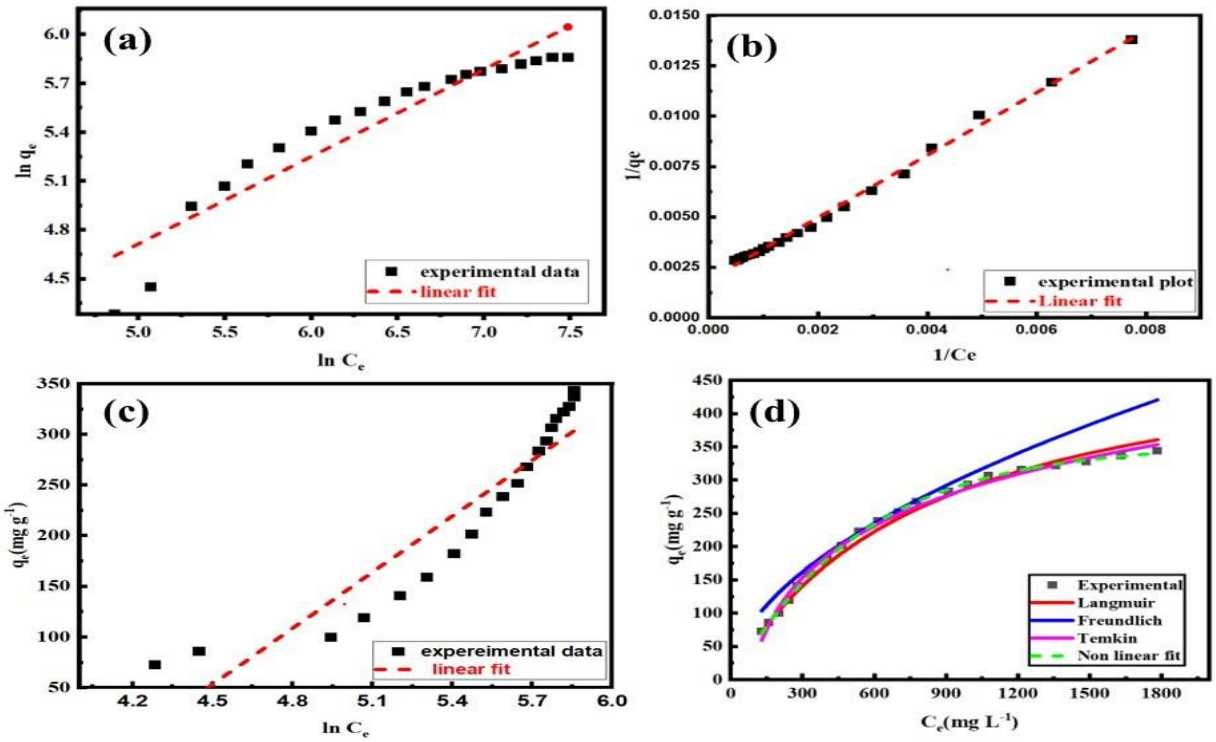

Fig. 8. Experimental data fit Lenear fit into (a) Freundlich (b) Langmuir and (c) Temkin isotherm models (d) Combined experimental non-linaer data fit into all three models

Table 2. Isotherm Parameters for different isotherm models adopted for the Adsorption of RG-19 dye on BMGG.

Isotherm model	Parameter	Value
Langmuir	q_{max}	526.31
	K_L	0.00122
	R^2	0.9955
Freundlich	K_F	7.663
	1/n	0.535
	R^2	0.88764
Temkin	A_T	0.0148
	B	184.478
	R^2	0.87106

4.4. Adsorption Thermodynamics

The spontaneity as well the endothermic or exothermic nature of the adsorption process on BMGG are predicted through thermodynamic parameters; ΔG^o, ΔS^o, and ΔH^o (Wen et al., 2022). These properties can be determined using equations 9 and 10:

$$\Delta G^o = -RTlnK_d \quad (9)$$

$$lnK_d = -\frac{\Delta S^o}{R} - \frac{\Delta H^o}{RT} \quad (10)$$

where R is the gas constant (8.314 J mol−1 K^{-1}), T (in K) is the temperature, K_d (in kJ mol−1) is the distribution coefficient ($K_d = q_e/C_e$), ΔG^o (in kJ mol−1) is the change in the Gibbs free energy, ΔS^0 (in J mol^{-1} K^{-1}) is the value of the entropy change, and ΔH^0 (in kJ mol^{-1}) is the enthalpy change at 298 K. As indicated by the values of ΔG^o, ΔS^o, and ΔH^o are shown in Table 3, ΔG^o value shows a decrease for the adsorption process in going from 298 K to 338 K. This agrees with the fact that an optimum temperature of 298 K is best for the adsorption to occur. Moreover, the exothermic behavior of the adsorption phenomenon along with a more orderly arrangement of the adsorbent surface during the interaction between the

BMGG surface and dye molecules are predicted respectively by the negative value of ΔH^o and a negative value of ΔS^o.

Table 3. Thermodynamic Parameters calculated for the Adsorption of RG 19 Dye on BMGG

Temperature (K)	ΔG^o (kJ mol^{-1})	ΔH^o (kJ mol^{-1})	ΔS^o (J mol^{-1})
298	-1.673	-10.018	-28.259
313	-1.050		
338	-0.512		

4.5. Recyclability studies

Reusability of a nanocomposite is a very important parameter in the aspect of its utility in real-life application (Ponce et al., 2022) The reusability of the as-synthesized bio-nanocomposites was analyzed through 8 repeating cycles of adsorption- desorption experiments on RG 19 dye. The study includes equilibrium adsorption of RG 19 on the adsorbent surface after which BMGG was separated with the help of an external magnet, then transferred into 0.1 M HCl solution and allow desorption to take place by keeping in an incubator shaker for 3 h at room temperature. The adsorbent was then washed with distilled water till a neutral pH and dried to be reused in the next adsorption cycle (Figure 9). Results show that the adsorption capacity values of RG 19 on BMGG still remain even after eight cycles of the desorption-adsorption process, which indicates excellent recovery capability and reusability of BMGG as an adsorbent material.

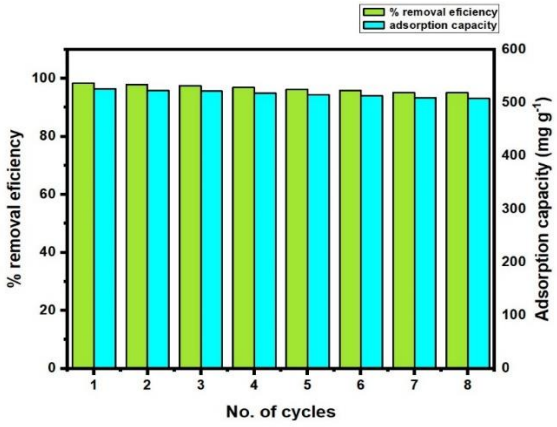

Figure 8. Recyclability data showing retention of removal efficiency of BMGG up to 8 adsorption-desorption cycles

Table 4. Comparison of maximum adsorption capacity of BMGG with other magnetic polysaccharide-based nanocomposites for dyes adsorption.

Sl. No.	Starting Polysaccharide	Material	Dye	Adsorption capacity (mg g^{-1})	Reference
1.	Guar gum	(Pc-cl-GG/SPION)	m-cresol o-chlorophenol	176.1 75.6	Sharma et al., 2017
2.	Guar gum	GG-LDH-Fe_3O_4 (GLF)	Methylene blue	84%	Tabatabaeian et al., 2021
3.	Cellulose	M3D–PAA–CCN	Methylene blue	332	Samadder et al., 2020
4.	Chitosan	MCS/GO-PEI	Congo Red	162.07	Kadam & Lee, 2015
5.	Chitosan	Chit-PVA/MgO/ Fe_3O_4	Remazol brilliant blue R	163.7	Jawad et al., 2022
6.	Chitosan	MCB	Amaranth dye	404.18	Wang et al., 2022
7.	Chitosan	$CaNiFe_2O_4$/Chitosan	Methylene blue	238	Ahmed et al., 2021
8.	Tragacanth gum	$ZnFe_2O_4$/SiO_2/Tragacanth gum magnetic nanocomposite	Congo Red	159.90	Etemadinia et al., 2019
9.	Inulin	magnetic inulin nanocomposite	Methylene blue	136.4	Herab et al., 2022
10.	κ-carrageenan	CKAlFe	Congo red Alizarin red	26.9 and 33.5	Shahinpour et al., 2022
11.	Carboxymethyl chitosan and acetoacetate cellulose	CMCht/OCAA	Methylene blue	564.64	Wang et al., 2022

12.	Chitosan	(CTS-TPP/MgO/Fe_3O_4	Reactive Blue 19	120.3	Jawad et al., 2022
13.	Guar Gum	BMGG	Reactive Green 19	526.32	This study

4.6. Adsorption Mechanism

The surface charge along with the nature of the functional groups on the synthesized material is pivotal in determining the nature of interactions between the nanomaterial and dye molecules. Hydrogen-bonding and electrostatic interactions are responsible for anionic dye adsorption on the surface of BMGG (Hussain et al., 2021). There are plenty of hydroxyl groups on the polymeric network of guar gum backbone which leads to extensive intermolecular hydrogen bonding with RG 19 dye molecules fostering their adsorption on BMGG. surface. Moreover, presence of highly electronegative nitrogen groups and aromatic rings in RG 19 structure reinforces the adsorption of these dye molecules on the positively charged surface of BMGG at a low pH through strong electrostatic interactions. As suggested by experimental studies, the pH_{ZPC} for BMGG is 7.1, which infers that the surface will be positively charged below 7.1 pH and negatively charged at pH higher than 7.1. This basically supports the preferential adsorption of anionic dyes (RG 19) by BMGG at a lower pH where the surface charge is positive. In the presence of excess of H^+ ions at lower pH, the hydroxyl groups may undergo protonation increasing the amount of positive charge on the adsorbent surface thereby facilitating the adsorption of anionic dyes. Fig. 9 shows all the possible interactions which act as the driving forces for the adsorptive removal of RG19 dye using BMMG and also illustrates how pH plays a key role on the establishment of a charged surface on the nanomaterial that subsequently becomes the basis of interaction between the adsorbate-adsorbent couple.

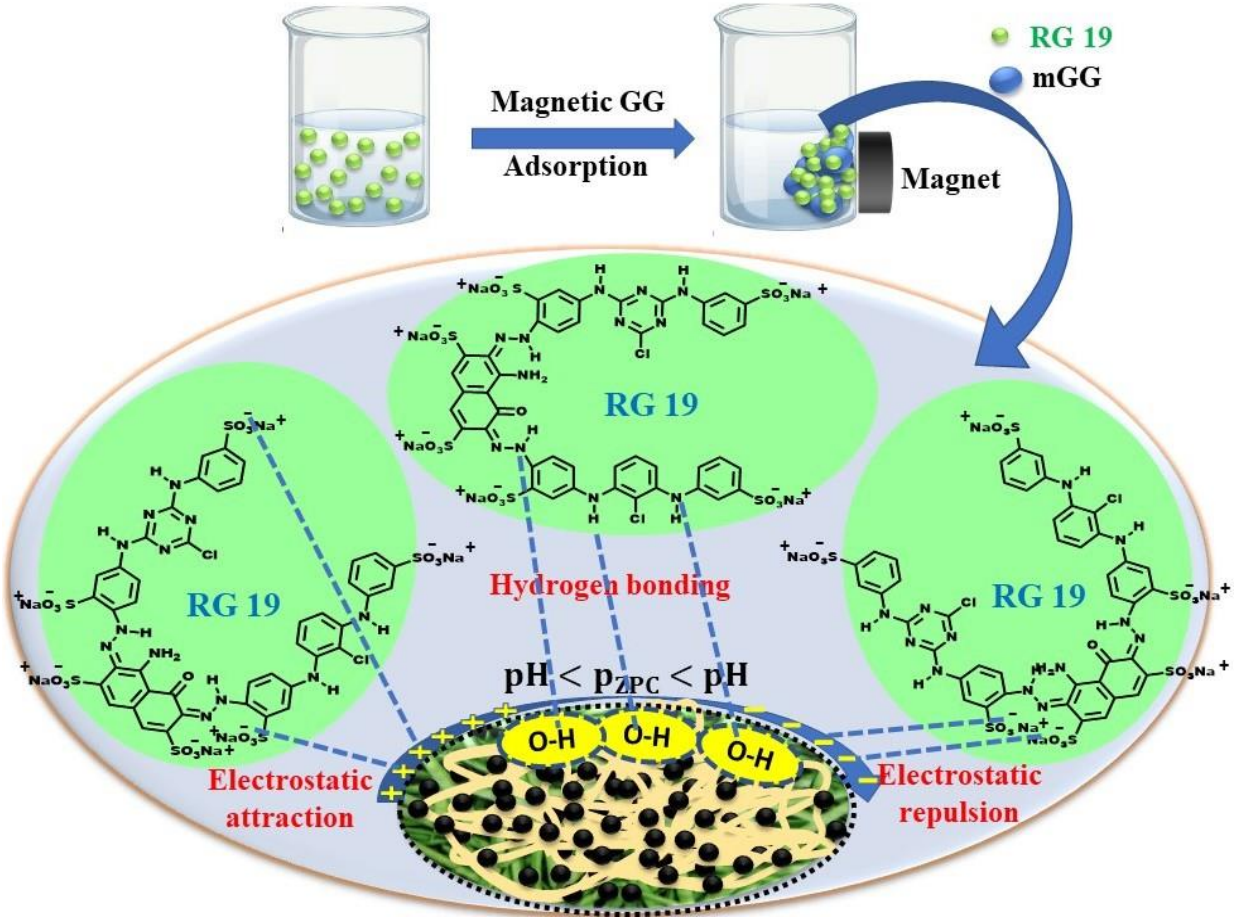

Fig. 9. Schematic diagram showing possible interactions between BMGG and RG 19 dyes at different pH

5. CONCLUSIONS

A promising adsorbent that shows preferentially excellent adsorption towards anionic reactive dyes (RG 19) was successfully designed via hydrothermal method. The material was characterized for its morphology and composition using various techniques. Compared to several other magnetic materials reported, BMGG. is observed to show improved performance towards anionic dye adsorption with a maximum adsorption capacity of 526.31 mg g^{-1}. Electrostatic and extensive hydrogen bonding interactions at a low pH are predicted to be the main driving forces in the adsorption process. Equilibrium adsorption data when fitted into several isotherm models suggested Langmuir model to be the best fit model that can describe the adsorption behavior indicating monolayer adsorption of RG 19 on the surface of BMGG. On the other hand, the kinetic behavior of the adsorption phenomenon can be best represented by the pseudo-second-order model. Results of thermodynamic studies confirmed the spontaneity and exothermic nature of the process. With these promising results, BMGG can be concluded to be an excellent adsorbent for anionic water contaminants with added advantage of easy separation and a guarantee cost-effective nature along with an easy fabrication method, that gives a great scope for its practical application in wastewater remediation.

Declaration of competing interest

The authors declare no competing financial interests that could have appeared to influence the work reported in this paper.

ACKNOWLEDGEMENTS

The authors are grateful to the Principals of Sri Venkateshwara College, University of Delhi and Acharya Narendra Dev College, University of Delhi for their perennial support and guidance. Authors would also like to extend their gratitude to the Head, Department of Chemistry, Manipur University, Canchipur, for his continuous cooperation and encouragement.

REFERENCE

[1] Ahmed, H.A.; Mubarak, M.F. (2021) Adsorption of Cationic Dye Using A Newly Synthesized CaNiFe2O4/Chitosan Magnetic Nanocomposite: Kinetic and Isotherm Studies. *J. Polym. Environ. 29*, 1835–1851.

[2] Alshahrani, A. A., Alorabi, A. Q., Hassan, M. S., Amna, T., & Azizi, M. (2022). Chitosan-Functionalized Hydroxyapatite-Cerium Oxide Heterostructure: An Efficient Adsorbent for Dyes Removal and Antimicrobial Agent. *Nanomaterials*, *12*(15), 2713. You, J., Liu, C., Feng, X., Lu, B., Xia, L., & Zhuang, X. (2022). In situ synthesis of ZnS nanoparticles onto cellulose/chitosan sponge for adsorption–photocatalytic removal of Congo red. *Carbohydrate Polymers*, *288*, 119332.

[3] Arabi, M., Ostovan, A., Ghaedi, M., & Purkait, M.K. (2016). Novel strategy for synthesis of magnetic dummy molecularly imprinted nanoparticles based on functionalized silica as an efficient sorbent for the determination of acrylamide in potato chips: optimization by experimental design methodology. *Talanta*, *154*, 526-532.

[4] Bagheri, A.R., Arabi, M., Ghaedi, M., Ostovan, A., Wang, X., Li, J., & Chen, L. (2019). Dummy molecularly imprinted polymers based on a green synthesis strategy for magnetic solid-phase extraction of acrylamide in food samples. *Talanta*, *195*, 390-400.

[5] Balan, V., Mihai, C. T., Cojocaru, F. D., Uritu, C. M., Dodi, G., Botezat, D., & Gardikiotis, I. (2019). Vibrational spectroscopy fingerprinting in medicine: from molecular to clinical practice. *Materials*, *12*(18), 2884.

[6] Banisheykholeslami, F., Hosseini, M., & Darzi, G. N. (2021). Design of PAMAM grafted chitosan dendrimers biosorbent for removal of anionic dyes: adsorption isotherms, kinetics and thermodynamics studies. *International Journal of Biological Macromolecules*, *177*, 306-316.

[7] Borousan, F., Yousefi, F., Ghaedi, M., 2019. Removal of malachite green dye using IRMOF-3–MWCNT-OH–Pd-NPs as a novel adsorbent: kinetic, isotherm, and thermodynamic studies. J. Chem. Eng. Data 64, 4801–4814.

[8] Cao, S. W., Zhu, Y. J., & Chang, J. (2008). Fe_3O_4 polyhedral nanoparticles with a high magnetization synthesized in mixed solvent ethylene glycol–water system. *New Journal of Chemistry*, *32*(9), 1526-1530.

[9] Cooper. P. (1995) The Problem of Colour, in "Colour in Dyehouse Effjuent," Society of Dyers and Colourists. Bradford. U.K.., pp. 9-14.

[10] Do, N. H., Truong, B. Y., Nguyen, P. T., Le, K. A., Duong, H. M., & Le, P. K. (2022). Composite aerogels of TEMPO-oxidized pineapple leaf pulp and chitosan for dyes removal. *Separation and Purification Technology*, *283*, 120200.

[11] Durairaj, K., Senthilkumar, P., Velmurugan, P., Divyabharathi, S., Kavitha, D. (2019). De-

[12] Durairaj, K., Senthilkumar, P., Velmurugan, P., Divyabharathi, S., & Kavitha, D. (2019). Development of activated carbon from Nerium oleander flower and their rapid adsorption of direct and reactive dyes. *International Journal of Green Energy*, *16*(7), 573-582.

[13] Etemadinia,T. Barikbin, B., Allahresani, A. (2019), Removal of Congo red dye from aqueous solutions using znfe2o4/sio2/Tragacanth gum magnetic nanocomposite as a novel adsorbent. Surfaces and Interfaces.14, .117-12.

[14] Gemici, B. T., Ozel, H. U., & Ozel, H. B. (2021). Removal of methylene blue onto forest wastes: Adsorption isotherms, kinetics and thermodynamic analysis. *Environmental Technology & Innovation*, *22*, 101501.

[15] Herab,A.A., Salari,D., Ostadrahimi, A., Olad, A. (2022) Preparation of magnetic inulin nanocomposite and its application in the removal of methylene blue and heavy metals from aqueous solution, Materials Chemistry and Physics, 291,2022,126580.

[16] Hossain, M.Y., Sarker, S., Zakaria, M., Islam, M.R., Fayazi, R.U., Acharjya, S. (2020). Influence of process parameters on exhaustion fixation and color strength in dyeing of cellulose fiber with reactive dye. Int. J. Textile Sci. Eng. 3, 127.

[17] Hussain, D., Khan, S. A., & Khan, T. A. (2021). Fabrication and characterization of mesoporous guar gum/NiWO4 nanocomposite for efficient adsorption of phloxine B and crystal violet from aqueous solution and evaluation of its antioxidant activity. *Colloid and Interface Science Communications*, *44*, 100488.

[18] Jawad, A. H., Sahu, U. K., Jani, N. A., ALOthman, Z. A., & Wilson, L. D. (2022). Magnetic crosslinked chitosan-tripolyphosphate/MgO/Fe3O4 nanocomposite for reactive blue 19 dye removal: Optimization using desirability function approach. *Surfaces and Interfaces*, *28*, 101698.

[19] Jawad, A.H., Hameed, B.H. & Abdulhameed, A.S. (2022). Synthesis of biohybrid magnetic chitosan-polyvinyl alcohol/MgO nanocomposite blend for remazol brilliant blue R dye adsorption: Solo and collective parametric optimization. *Polym. Bull.* 6, https://doi.org/10.1007/s00289-022-04294-

[20] Kadam, A.A., Lee, D.S. (2015). Glutaraldehyde cross-linked magnetic chitosan nanocomposites: Reduction precipitation synthesis, characterization, and application for removal of hazardous textile dyes. Bioresource technology, 193, 563-567.

[21] Lee, C.H., Tang, A.Y.L., Wang, Y., Kan, C.W. (2019). Effect of reverse micelle-encapsulated reactive dyes agglomeration in dyeing properties of cotton. Dyes Pigment 161, 51–57.

[22] Lewis. D. M. (1993). New Possibilities to Improve Cellulosic Fibre Dyeing Processes with Fibre-Reactive Systems, J. Soc. Dyers Colour. 109 (11), 357-364

[23] Li, S., Zhang, T., Tang, R., Qiu, H., Wang, C., & Zhou, Z. (2015). Solvothermal synthesis and characterization of monodisperse superparamagnetic iron oxide nanoparticles. *Journal of Magnetism and Magnetic Materials*, *379*, 226-231.

[24] Liu, X., Wang, Y., Smith, R. L., Fu, J., & Qi, X. (2021). High-capacity structured MgO-Co adsorbent for removal of phosphorus from aqueous solutions. *Chemical Engineering Journal*, *426*, 131381.

[25] Mahmoud A. S., Ghaly, A. E., & Brooks, M. S. (2007). Removal of dye from textile wastewater using plant oils under different pH and temperature conditions. American Journal of Environmental Sciences, 3, 205–218.).

[26] Malfait, T., Van Dael, H., & Van Cauwelaert, F. (1989). Molecular structure of carrageenans and kappa oligomers: A Raman spectroscopic study. *International journal of biological macromolecules*, *11*(5), 259-264.

[27] Mudgil, D., Barak, S., & Khatkar, B. S. (2012). X-ray diffraction, IR spectroscopy and thermal characterization of partially hydrolyzed guar

gum. *International Journal of Biological Macromolecules*, *50*(4), 1035-1039.

[28] Narayanamma, A., & Raju, K. M. (2016). Development of guar gum based magnetic nanocomposite hydrogels for the removal of toxic Pb2+ ions from the polluted water. *Int. J. Sci. Res*, *5*, 1588-1595.

[29] Noval, V. E., & Carriazo, J. G. (2019). Fe_3O_4-TiO_2 and Fe_3O_4-SiO_2 core-shell powders synthesized from industrially processed magnetite (Fe_3O_4-microparticles. *Materials Research*, *22*.

[30] Özacar, M., & Sengil, I. A. (2003). Adsorption of reactive dyes on calcined alunite from aqueous solutions. Journal of Hazardous Materials, 98, 211–224. Özacar, M., & Sengil, I. A.

[31] Pati, S. S., Mahendran, V., & Philip, J. (2013). A simple approach to produce stable ferrofluids without surfactants and with high temperature stability. *Journal of Nanofluids*, *2*(2), 94-103.

[32] Ponce, J., Peña, J. U. A. N., Roman, J., & Pastor, J. M. (2022). Recyclable photocatalytic composites based on natural hydrogels for dye degradation in wastewaters. *Separation and Purification Technology*, *299*, 121759.

[33] Samadder, R.; Akter, N.; Roy, A.C.; Uddin, M.; Hossen, J.; Azam, S. (2020). Magnetic nanocomposite based on polyacrylic acid and carboxylated cellulose nanocrystal for the removal of cationic dye. RSC Adv., 10, 11945–11956.

[34] Saya, L., Gautam, D., Malik, V., Singh, W.R., Hooda, S. (2021**).** Natural Polysaccharide Based Graphene Oxide Nanocomposites for Removal of Dyes from Wastewater: A Review. *Journal of Chemical and Engineering Data*, *ACS*, 66, 11-37

[35] Saya, L., Malik, V., Singh, A., Singh, S., Gambhir, G., Singh, W. R., Chandra, R., Hooda, S. (2021). Guar gum-based nanocomposites: Role in water purification through efficient removal of dyes and metal ions. *Carbohydrate Polymers*, *261*, 117851.

[36] Shahinpour, A., Tanhaei, B., Ayati, A., Beiki, H., Sillanpää, M. (2022) Binary dyes adsorption onto novel designed magnetic clay-biopolymer hydrogel involves characterization and adsorption performance: Kinetic, equilibrium, thermodynamic, and adsorption mechanism, Journal of Molecular Liquids, 366, 20303,

[37] Tabatabaeian, R., Dinari, M., Aliabadi, H.M. (2021). Cross-linked bionanocomposites of hydrolyzed guar gum/magnetic layered double hydroxide as an effective sorbent for methylene blue removal, C*arbohydrate Polymers, 257*, 117628.

[38] Verma, M., Tyagi, I., Kumar, V., Goel, S., Vaya, D., & Kim, H. (2021). Fabrication of GO–MnO2 nanocomposite using hydrothermal process for cationic and anionic dyes adsorption: Kinetics, isotherm, and reusability. *Journal of Environmental Chemical Engineering*, *9*(5), 106045.

[39] Wang, F., Huang, K., Xu, Z., Cao, F., Chen, C., Shi, F., & Chen, N. (2022). Preparation of high-strength dynamic polysaccharide nanocomposite hydrogels and their application towards dye adsorption. *Industrial Crops and Products*, *189*, 115704.

[40] Wang, F., Li, L., Iqbal, J., Yang, Z, Du, Y. (2022) Preparation of magnetic chitosan corn straw biochar and its application in adsorption of amaranth dye in aqueous solution. *International Journal of Biological Macromolecules*,199,234-242.

[41] Wen, Y., Xie, Z., Xue, S., Li, W., Ye, H., Shi, W., & Liu, Y. (2022). Functionalized polymethyl methacrylate-modified dialdehyde guar gum containing hydrazide groups for effective removal and enrichment of dyes, ion, and oil/water separation. *Journal of Hazardous Materials*, *426*, 127799.